

Quasichemical approximation in binary alloys

A. Sher and Mark van Schilfgaarde
SRI International, Menlo Park, California 94025

An-Ban Chen and William Chen
Department of Physics, Auburn University, Alabama 36849
 (Received 10 March 1987)

In this theoretical study, the quasichemical approximation for an $A_{1-x}B_x$ alloy is formulated for an arbitrary lattice and choice of cluster. The statistical problem of the average number of each class of clusters is collapsed into a polynomial equation. An n -atom cluster of type j is characterized by an excess energy ϵ_j , the number of B atoms $n_j(B)$ and a degeneracy g_j . If ϵ_j is a linear function of $n_j(B)$ and g_j is a binomial coefficient of n and $n_j(B)$, then the cluster populations are random. Strains due to lattice-size mismatches, chemical (electron-ion interaction) differences, and differences between the electron-electron Coulomb interactions of the alloy constituents drive nonlinear variations of ϵ_j on $n_j(B)$. The g_j is modified by coherent, externally applied stresses and temperature gradients present during crystal growth. We derive the conditions under which compounds are formed or spinodal decomposition occurs. We also discuss the possibility of materials consisting of arrays of two kinds of domains: one a random alloy and the other an ordered compound. The theory is specialized to semiconductor alloys $A_{1-x}B_xC$ in a distorted zinc-blende structure; numerical results are presented for $\text{Ga}_{1-x}\text{In}_x\text{As}$ and $\text{GaAs}_{1-x}\text{Sb}_x$ alloys. A major conclusion is that semiconductor alloys are almost never truly random.

I. INTRODUCTION

In a binary alloy $A_{1-x}B_x$ or alloy $A_{1-x}B_xC$, the A and B atoms assume some configuration on a crystalline lattice.¹ Computation of the partition function divides naturally into the statistical part, i.e., the number of ways to configure the A and B atoms on the lattice with a given energy, and the computation of the energies themselves.^{2,3} It is well known that precise computation of the statistics is notoriously difficult, even for the simplest of Hamiltonians.⁴⁻⁷ For realistic Hamiltonians, an alloy is usually approximated as an ensemble of statistically independent, few-atom clusters. In the so-called cluster approximations, the lattice is (arbitrarily) divided into clusters of small size. In the fcc lattice, for example, a popular choice of cluster is the tetrahedron of four atoms, in which case the possible "species" of clusters^{2,8-10} are A_4 , A_3B , A_2B_2 , AB_3 , and B_4 . The Hamiltonian must be so constructed that the energy of each cluster is independent of its environment. In general, this requires some approximation to the true Hamiltonian. Because the choice of cluster affects both the statistics and the energetics, the approximations for these two aspects of the theory are closely linked and must be treated on an equal footing. This point has not been fully appreciated, and one aim of the present work is to illustrate its significance.

We formulate the partition function Z for an arbitrary lattice and cluster in the general quasichemical approximation, the simplest of the cluster approximations. We shall demonstrate that for the special case of the zinc-blende lattice, the combinatorial analysis reduces identically to results¹⁰ obtained from an early version of the cluster variation method of Kikuchi.¹¹ The statistical

problem then collapses into a single polynomial equation whose solution yields a chemical potential that constrains the average number of A (or B) atoms to a fixed value.² All thermodynamic quantities, including the mixing enthalpy and the cluster populations, are essentially trivially obtained once the chemical potential is known. Although we shall formulate the theory generally, we will focus on the tetrahedrally coordinated zinc-blende lattice, for which the quasichemical approximation (QCA) is particularly suited. Besides the thermodynamic quantities, our theory yields information about local correlation, e.g., the distribution of atoms and local bond lengths within clusters. Our results show that a realistic semiconductor alloy is never truly random. This information is important for studying alloy properties that are sensitive to the local environment, such as local phonon modes, defects, NMR spectra, and the like.

A genuine QCA is equivalent to a grand ensemble of clusters in equilibrium with the alloy as a reservoir. The distribution of different cluster configurations is governed by the cluster energy, the number of A (or B) atoms, and the degeneracy. Because QCA is strictly correct only for homogeneous alloys and does not properly account for all statistical correlations among clusters, its applicability has limits. However, the theory can be extended with additional approximations to inhomogeneous phases. All pseudobinary alloys grown from equilibrium processes are believed to fall within the scope of this theory. To optimize the accuracy of the predictions, the cluster size should be comparable to the correlation length in the alloy. Thus caution must be exercised in applying QCA predictions to alloys with long-range order. However, for a given cluster size, the energy and the statistics are treated on an equal

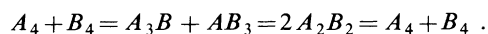
footing. A related cluster approximation, the cluster variation method (CVM) of Kikuchi,^{5,6} represents an improvement over QCA in the statistical counting of the number of cluster arrangements corresponding to a given alloy energy, in which some statistical correlations between clusters are included. Therefore, CVM is more precise for alloys in which long-range correlation is important, e.g., systems near the order-disorder transition. For general lattice structures, however, the solution in CVM is considerably more difficult than our present formulation of the QCA. The far simpler QCA is to be preferred in those instances where the counting schemes in CVM and QCA are equivalent (e.g., pair clusters), the Hamiltonian is sufficiently crude that errors in the statistical approximation are not significant, or the long-range order is not important. The physically important zinc-blende lattice with five-atom, 16-bond clusters proves to be one of the exceptional cases in which QCA and CVM yield identical results.

For an alloy with long-range order, there is an additional complication beside the combinatorial analysis. There are extra many-body long-range contributions to the total energy of the alloy that are not simply expressed as a sum of cluster energies. These extra energy contributions arise from electron-electron Coulomb interactions that are enhanced by Madelung sums.⁴ A way to treat this problem is as a nearly perfect crystal, for which band-structure techniques work best. The disorder may then be treated as a perturbation. Some recent calculations^{8,12} on semiconductor alloy statistics have adopted a hybrid procedure that uses the cluster energy obtained from a "crystalline" calculation, but employs the cluster statistics—the CVM. Because this approach includes long-range effects, it is doubtful that it accurately describes disordered phases of an alloy, but it should be useful near and below order-disorder transition temperatures where long-range order is present. This paper presents details of the quasichemical approximation in Sec. II. Section III concentrates on pseudobinary semiconductor alloys, and Sec. IV presents concluding remarks.

II. STATISTICAL THEORY

A. Quasichemical approximation and constraints

We use the term *quasichemical approximation* (QCA) in a precise sense, namely that the crystal is (arbitrarily) divided into an ensemble of clusters each of which is taken to be independent—statistically and energetically—of the surrounding configuration. The term originally derives from a treatment of the lattice as a series of chemical reactions between clusters. In the example of the four-atom tetrahedron, there are three reactions:



The mass-action equations (three in this case) and the two constraints that fix the number of *A* and *B* atoms determine the concentration of the different molecular species. Our formalism can be shown to be equivalent to this point of view; it makes evident the essential nature of the assumption the QCA embodies.

The essence of the QCA is the assumption of statistical independence of the different clusters. We shall first derive a combinatorial formula in this approximation. Using the method of steepest descents, we exploit our particular form of the combinatorial expression to collapse the partition function into a single polynomial for an effective activity coefficient, which bears a simple relation to the chemical potential. All cluster approximations constrain the material to be spatially homogeneous everywhere. To describe a spatially inhomogeneous alloy in a cluster approximation, the free energy must be minimized with respect to the relative populations of the various compositions, subject to the constraints that the total number of atoms is fixed and the population distribution yields the correct composition.

Consider a lattice of *N* sites on which the *A* and *B* atoms assume some configuration. If the alloy composition is expressed as $A_{1-x}B_x$, the numbers of *A* and *B* atoms are $N_A = (1-x)N$ and $N_B = xN$. We first decompose the lattice into *M* *n*-atom microclusters, which will be treated independently. We classify the various species of microclusters into groups of distinct cluster energies ϵ_j . For a particular configuration of the entire lattice, there are M_j clusters of energy ϵ_j , with $M = \sum_j M_j$. This can also be written as

$$\sum_j x_j = 1 , \quad (1)$$

where $x_j = M_j/M$ is the fraction of clusters of energy ϵ_j . The index $j=0, 1, \dots, J$ ranges over the different species of microclusters identified by energy ϵ_j , the number of *A* and *B* atoms [$n_j(A)$, $n_j(B)$, respectively], and degeneracy g_j . There is additionally a constraint on the composition:

$$\sum_j n_j(A)x_j = nN_A/N = n(1-x) , \quad (2a)$$

or

$$\sum_j n_j(B)x_j = nN_B/N = nx . \quad (2b)$$

To give an example, consider the tetrahedron of four atoms in the fcc lattice. In the absence of forces breaking the cubic symmetry, there are five distinct cluster energies, ϵ_j , depending only on the number of *A* atoms, $j=0, 1, 2, 3$, or 4. The number of distinguishable ways, g_j , of arranging the *A* or *B* atoms on the four sites are $g_j = 1, 4, 6, 4$, and 1 for $j=0, 1, 2, 3, 4$. These degeneracies can be split by mechanisms that lower the symmetry, such as a coherent strain, in which case the number of distinct energies would increase. In general, the g_j must satisfy $\sum_j g_j = 2^n$. In this example the number of clusters *M* equals the number of atomic sites $M = N$.

B. Partition function

In a cluster approximation, the partition function *Z* can be written generally as

$$Z(\{M_j\}) = \sum_{\{M_j\}}^{(1,2)} G(\{M_j\}) e^{-E(\{M_j\})/kT} , \quad (3)$$

where $E(\{M_j\})$ is the energy of the solid configured with

the set of microclusters $\{M_j\} = M_0, M_1, \dots$ and can be written

$$E(\{M_j\}) = \sum_j M_j \varepsilon_j. \quad (4)$$

Equation (4) follows from the second assumption of the QCA, that the energy of each cluster is independent of its environment. The superscript on the sum in Eq. (3) indicates that the set $\{M_j\}$ is constrained to satisfy Eqs. (1) and (2). $G(\{M_j\})$ is the number of ways to configure the alloy with the set of $\{M_j\}$ microclusters. The number of configurations $G(\{M_j\})$ is the total number of ways in which N_A indistinguishable atoms and N_B indistinguishable atoms can be placed on N sites, multiplied by the fraction of all configurations with N_A and N_B atoms that have $\{M_j\}$ microclusters. The QCA to G can be obtained in terms of the variables x_j^0 , defined to be the fraction of microclusters of type j found in all possible configurations of N_A and N_B atoms. That is,

$$x_j^0 = g_j x^{n_j(B)} (1-x)^{n_j(A)}, \quad (5)$$

where $n_j(B)$ and $n_j(A)$ are the number of B and A atoms, respectively, with $n = n_j(B) + n_j(A)$. Here, x_j^0 is obtained from a product of the separate independent probabilities of finding a specified atom at a given site.

With the assumption that the various clusters are independent, the joint probability of finding the set of $\{M_j\}$ clusters factors into a simple product of the separate probabilities x_j^0 , so that

$$G(\{M_j\}) \approx \frac{N!}{N_A! N_B!} \left[\frac{M!}{\prod_j M_j!} \prod_j (x_j^0)^{M_j} \right]. \quad (6)$$

$\prod_j (x_j^0)^{M_j}$ is the probability of finding a given set of clusters $\{M_j\}$ in the lattice, and $M! / \prod_j M_j!$ is the number of distinguishable ways of arranging that set of clusters on M sites. This is a general statement of the quasichemical approximation, or QCA.

If the total energy $E(\{M_j\})$ were improved from that expressed by Eq. (4) to include cluster-cluster interactions of the form $\frac{1}{2} M \sum_{j,j'} \varepsilon_{jj'} x_j x_{j'}$, where $x_j = M_j / M$, then it would also be necessary to modify the expression for $G(\{M_j\})$. In this case, a more complex version of the Kirkuchi expression for $G(\{M_j\})$ would be more appropriate than the one we are using. However, there is no justification for inserting a more complete expression for G into the partition function without the corresponding modification of $E(\{M_j\})$, since the physical interpretation of G is that it is the number of ways the clusters can be arranged to reach the energy E . It is intuitively obvious that, as the cluster size increases, typical energy ratios $\varepsilon_{j,j'} / \varepsilon_j$ will become progressively smaller.

If one defines an entropy $S \equiv k \ln G$, then this entropy becomes

$$\begin{aligned} S &= -kN \left[(1-x) \ln(1-x) + x \ln x + \sum_j (x_j \ln x_j - x_j \ln x_j^0) \right] \\ &= kN \left[3[(1-x) \ln(1-x) + x \ln x] - \sum_j x_j \ln(x_j / g_j) \right]. \end{aligned} \quad (7)$$

The second form of Eq. (7) is identical with that derived from an early version of the CVM (Ref. 11) for a zincblende lattice [see Eq. (5) in Ref. 11]. The first form of Eq. (7) differs from that of Czyzyk *et al.*,⁸ who have $x_j^0 \ln x_j^0$ in the final term in place of our $x_j \ln x_j^0$. Notice that for a random alloy in which $x_j = x_j^0$, Eq. (7) reduces to the regular solution model expression.

An instructive special case is the classic Bethe-Peierls approximation.⁷ It uses a two-atom cluster and three species (AA , AB , and BB bonds), with $n_j(B) = j$. Then Eq. (6) becomes

$$G = \frac{N!}{N_A! N_B!} \left[\frac{M!}{M_{AA}! M_{AB}! M_{BB}!} x^{2M_{AA}} \times [2x(1-x)]^{M_{AB}} (1-x)^{2M_{BB}} \right], \quad (8)$$

and can be shown to be identical, in the limit of large N , with the Bethe-Peierls approximation, the classical QCA,⁷ and the cluster variation statistics for arbitrary coordination number z_c .

Returning to the QCA, the partition function can be expressed as

$$\begin{aligned} Z &= \frac{1}{2\pi i} \frac{N!}{N_A! N_B!} \oint d\xi \xi^{-(nM+1)} \\ &\quad \times \left[\sum_{\{M_j\}}^{(1)} M! \prod_j \frac{(x_j^0 \xi^{n_j(B)} e^{-\varepsilon_j/kT})^{M_j}}{M_j!} \right], \end{aligned} \quad (9)$$

where the constraint of Eq. (2) has been incorporated into Z as a Kronecker delta, represented as a Cauchy integral:

$$\delta\left(\sum_j n_j(B) M_j, nM\right) = \frac{1}{2\pi i} \oint d\xi \xi^{-\left[\sum_j n_j(B) M_j - nM + 1\right]}. \quad (10)$$

The summation in large parentheses in Eq. (9) can be performed exactly to yield

$$Z = \frac{1}{2\pi i} \frac{N!}{N_A! N_B!} \oint d\xi \xi^{-(nM+1)} \left[\sum_j x_j^0 \xi^{n_j(B)} e^{-\varepsilon_j/kT} \right]^M. \quad (11)$$

Equation (11) is most easily shown to be equivalent to Eq. (9) by expanding the sum over j repeatedly with the binomial theorem.

Because the integrand of Eq. (11) is highly peaked at its maximum (actually, the complex plane shows a sharp saddle point), we can employ the customary arguments¹³ in the method of steepest descents to evaluate the Cauchy integral. Define μ_B as

$$\frac{x \xi_{\max}}{1-x} \equiv e^{\mu_B/kT}. \quad (12)$$

The location of the saddle point introduces a constraint

equation on the average populations $\{\bar{x}_j\}$, so that μ_B must satisfy

$$nx = \overline{n_j(B)} = \frac{kT}{q} \frac{\partial q}{\partial \mu_B} = \sum_j n_j(B) g_j e^{[n_j(B)\mu_B - \varepsilon_j]/kT} / q, \quad (13)$$

where the "single cluster" grand partition function is

$$q \equiv \sum_j g_j e^{[n_j(B)\mu_B - \varepsilon_j]/kT}. \quad (14)$$

Z is then evaluated to an excellent approximation as

$$Z = \frac{N!}{N_A! N_B!} [q(1-x)^{n(1-x)} x^{nx} e^{-nx\mu_B/kT}]^M. \quad (15)$$

Equation (13) is a polynomial of order n in the unknown $e^{\mu_B/kT}$. Once this equation is solved for μ_B , the partition function and all thermodynamic quantities are simply obtained. With the substitution of Eq. (12), q manifestly has the form of the grand partition function for a single cluster, with μ_B the chemical potential for the B species. Here, μ_B and $\oint d\xi$ are intimately related because both impose the constraint, Eq. (2), that fixes the number of B species. This differs from the usual quasi-chemical treatment⁷ where a separate chemical potential is assigned for each cluster species, so that there are n polynomial equations to be solved simultaneously.

C. Helmholtz free energy

Because the volume dependence on alloy composition is negligible, the Helmholtz free energy F is essentially interchangeable with the Gibbs free energy; we shall work with F . In the QCA the free energy is

$$\begin{aligned} F(x, T) &= -kT \ln Z \\ &= Mn x \mu_B \\ &\quad + kT(N - Mn)[x \ln x - (1-x) \ln(1-x)] - M \ln q. \end{aligned} \quad (16)$$

D. Population distributions

It is evident from Eqs. (3) and (4) that the expectation values of the M_j are

$$\bar{M}_j = -kT \frac{\partial \ln Z}{\partial \varepsilon_j}. \quad (17)$$

With the aid of Eqs. (12)–(15), the average probability \bar{x}_j of finding cluster j can be expressed as

$$\bar{x}_j = \bar{M}_j / M = g_j \exp\{[n_j(B)\mu_B - \varepsilon_j]/kT\} / q, \quad (18)$$

which is evident from Eq. (14) if q is recognized as the cluster grand partition function.

While the total energy of a cluster ε_j is the quantity that enters into Eqs. (13), (14), and (18) for the average cluster populations \bar{x}_j , we shall demonstrate that only the excess energies Δ_j actually influence the population distributions. Define the excess energy relative to the energies

$\varepsilon_A, \varepsilon_B$ of an n -atom cluster composed of all A atoms in an AC host (or all B atoms in a BC host) as

$$\Delta_j = \varepsilon_j - (1-x)\varepsilon_A - x\varepsilon_B. \quad (19)$$

Since Eq. (19) amounts to changing a constant reference energy for a given x , Eqs. (13), (15), and (18), are left unchanged, except that Δ_j replaces ε_j and the free energy in Eq. (16) becomes the excess free energy. Thus only excess energies drive the cluster populations. Rather than introducing extra notation, we shall continue to use the symbol ε_j in Eqs. (13), (15), and (18) but we now refer to it as the *excess energy*. The excess energies evaluated numerically in Sec. III will be denoted as Δ_j because they are the differences given by Eq. (19). Since Δ_j is calculated directly, the accuracy of our results is not limited by taking a small difference between two poorly known large numbers.

It is also worth noting that if, in Eq. (19), ε_A and ε_B are replaced by the equivalent quantities ε_0 and ε_J in the alloy and they are weighted by the number of appropriate species in the cluster, then the populations $\{\bar{x}_j\}$ depend only on the differences

$$\Delta'_j = \varepsilon_j - \frac{n_j(A)}{n} \varepsilon_0 - \frac{n_j(B)}{n} \varepsilon_J, \quad (20)$$

but with a different chemical potential, $\mu'_B \equiv \mu_B - (\varepsilon_J - \varepsilon_0)/n$. It is occasionally instructive to keep this fact in mind. In particular, we always have $\Delta'_0 = \Delta'_J = 0$, so there are only $J-2$ nonvanishing Δ'_j energies.

E. Random distribution

One instructive special case is the case in which the ε_j is linear in $n_j(B)$, i.e., $\varepsilon_j = \varepsilon_0 + (\Delta\varepsilon)n_j(B)$ for constants ε_0 and $\Delta\varepsilon$. The total energy of the lattice is independent of the cluster populations M_j because the exchange of two alloy atoms from different clusters changes the energy of each cluster by an equal and opposite amount. [Any change in configuration that satisfies the constraint of Eq. (2) can be broken down into a sequence of exchange of atom pairs.] Expectation values \bar{x}_j will, therefore, be governed completely by the entropy and will be identical to the cluster populations of the random alloy, given in the QCA by Eq. (5). The nonlinearity in the cluster energies is thus a measure of the degree of nonrandomness a distribution will exhibit. This is proved in the QCA by finding a value of μ_B that satisfies the constraint in Eq. (13) and also makes the \bar{x}_j equal to the x_j^0 . Making the ansatz that μ_B satisfies

$$\frac{x}{1-x} = e^{-(\mu_B - \Delta\varepsilon)/kT},$$

then, using Eq. (5) and the relation $\sum_j x_j^0 = 1$, it is easily shown that

$$q = e^{-\varepsilon_0/kT} \sum_j g_j e^{n_j(B)(\mu_B - \Delta\varepsilon)/kT} = e^{-\varepsilon_0/kT} (1-x)^{-n},$$

and that Eq. (18) reduces to Eq. (5). The constraint, Eq. (13), becomes

$$nx = \sum_j n_j(B) x_j^0,$$

which is obviously satisfied, showing that the ansatz is correct. The free energy in this example is

$$F = NkT[x \ln x + (1-x) \ln(1-x)] + \varepsilon_0 + nx \Delta \varepsilon, \quad (21)$$

which is the entropy of a random alloy plus a concentration-weighted average of the internal energy of the pure materials.

F. Nonrandom distributions caused by coherent strains

We have demonstrated in Sec. II E that as long as ε_j is a linear function of $n_j(B)$ [no matter how large $d\varepsilon_j/dn_j(B)$ may be] and the degeneracy g_j is not lifted, then the alloy will always be driven by the entropy terms into a random distribution. However, if ε_j is a nonlinear function of $n_j(B)$ or g_j is lifted, then the atoms in the alloy will experience some correlations.

There are several mechanisms that cause ε_j to be nonlinear functions of $n_j(B)$. The principal ones we have identified to date are strains caused by lattice constant differences between the *AC* and *BC* constituents, potential differences between the constituents that cause "chemical shifts" in ε_j , and local electron-electron and Madelung interactions driven by charge shifts between the anions and cations. One mechanism that lifts the degeneracy is a long-range coherent strain field introduced by an externally applied stress. One practical example of a case in which there is a large stress source is an epitaxial layer grown on a substrate with a lattice mismatch. In the following sections mechanisms that cause nonlinearities in ε_j and their consequences on \bar{x}_j will be treated quantitatively, but here we shall examine a simple model to illustrate the nature of the effects caused by lifting the degeneracy g_j .

First, examine the classic Bethe-Peierls two-atom cluster mentioned earlier. Then, in the case normally treated, we have $J=2$, $j=n_j(B)=0,1,2$, $g_j=1,2,1$, and $\varepsilon_j=\varepsilon_0, \varepsilon_1, \varepsilon_2$. As we have demonstrated in the argument leading to Eq. (21), if $\varepsilon_j=\varepsilon_0+(\Delta\varepsilon)j$, then $\bar{x}_j=x_j^0$, and the distribution is random. We now examine a case where the degeneracy of the state $n_j(B)=1$ is split by an energy 2δ . Here, in our notation, $J=3$ and for $j=0,1,2,3$ we have $n_j(B)=0,1,1,2$, $g_j=1,1,1,1$, and $\varepsilon_j=\varepsilon_0, \varepsilon_0+\Delta-\delta, \varepsilon_0+\Delta+\delta$, and $\varepsilon_0+2\Delta$. Putting these values into Eqs. (13), (14), and (16) yields

$$\bar{x}_0 = (1-x)^2 \frac{1}{W[(1-x)\cosh\delta + xW]}, \quad (22a)$$

$$\bar{x}_1 = x(1-x) \frac{e^\delta}{(1-x)\cosh\delta + xW}, \quad (22b)$$

$$\bar{x}_2 = x(1-x) \frac{e^{-\delta}}{(1-x)\cosh\delta + xW}, \quad (22c)$$

$$\bar{x}_3 = x^2 \frac{W}{(1-x)\cosh\delta + xW}, \quad (22d)$$

where

$$W(x, \delta) \equiv \frac{(2x-1)\cosh\delta + [1-(2x-1)^2\sinh^2\delta]^{1/2}}{2x}. \quad (23)$$

First, note that when $\delta=0$, $W(x,0)=(2x-1)/2x$, and \bar{x}_j becomes the expected random population distribution. It is useful to define the ratio (a short-range order parameter)

$$r(x, \delta) \equiv \frac{\bar{x}_1 + \bar{x}_2}{\bar{x}_0 + \bar{x}_3} = \frac{2x(1-x)\cosh\delta}{\frac{(1-x)^2}{W} + Wx^2}. \quad (24)$$

This quantity serves as an indicator of the trends in the overall order. If $r(\frac{1}{2}, \delta) < 1$, there is a tendency toward spinodal decomposition; $r(\frac{1}{2}, \delta) = 1$ is indicative of a random alloy, and $r(\frac{1}{2}, \delta) > 1$ indicates a tendency towards the formation of a long-range ordered compound.

Examining two cases

$$W(x, 0) = 1$$

so that

$$r(x, 0) = \frac{2x(1-x)}{(1-x)^2 + x^2} \quad \text{and} \quad r(\frac{1}{2}, 0) = 1,$$

and

$$W(\frac{1}{2}, \delta) = 1 \quad \text{so that} \quad r(\frac{1}{2}, \delta) = \cosh\delta \geq 1$$

demonstrates that any splitting of the degeneracy in this pair interaction case always causes a tendency toward compound formation. There is no circumstance where there is tendency toward spinodal decomposition.

We have also examined the case of five-atom clusters in a zinc-blende crystal structure with a uniaxial strain in the (111) direction, and found that in the limit of large strains, the degeneracy splitting again always tends to form long-range ordered compounds. This tendency toward compound formation is, in fact, independent of the geometry. Any strain field that splits the degeneracy must decrease the energy of some configuration with a given $n_j(B)$ relative to other possible configurations. If the splitting is large enough, the favored configuration's population will grow at the expense of all others, so that an ordered compound is the preferred arrangement. This predicted tendency is in agreement with recent experiments¹⁴ in which a $\text{Si}_{1-x}\text{Ge}_x$ ($x=0.5$) was grown epitaxially on a Si substrate and the resulting layer was found to be ordered rather than random.

G. Spatial fluctuations

The free energy in a cluster approximation has no freedom for allowing spatial fluctuations in the cluster populations \bar{x}_j . Practical calculations of phase diagrams and other thermodynamic quantities must provide for this additional freedom in some approximate way. The approximation most commonly used implicitly is to express the free energy as the cluster approximation free energy at the local composition $x(r)$. In this approximation

$$F = \int d^3r F[x(r)], \quad (25)$$

where $F[x(r)]$ is the cluster approximation $F(x)$ to the

free energy evaluated at the "local" composition $x(r)$ and the integral is over a "unit volume." The average composition is constrained to be $\int d^3r x(r) = x$. Approximations to the free-energy functional more sophisticated than Eq. (21) are necessary to treat important classes of problems, such as concentration waves or other fluctuations.^{15,16} Sophistication, however, requires more information than is available in the cluster approximation to the free energy, and will not be considered here in detail.

III. PSEUDOBINARY SEMICONDUCTOR ALLOY

The pseudobinary alloy in the zinc-blende structure (in which the alloy atoms occupy the fcc sublattice¹) serves as an excellent practical illustration of the key points of this paper. This example, with relatively simple changes to the statistics, is also suitable for simple binary alloys, e.g., $\text{Si}_{1-x}\text{C}_x$, on a diamond lattice. In many of the alloys, the incoherent strain fields are believed to be the principal origin of the alloy mixing enthalpy, and we shall model the Hamiltonian with a force constant model. Such a model has a basis in Harrison's tight-binding bond-orbital approximation,^{17,18} which treats each two-center bond as uncoupled from the neighboring bonds. Harrison's metallization corrects the bond-orbital approximation for coupling between the bonds; we include that correction here as the so-called *chemical* terms. We have used this Hamiltonian previously,^{3,19} and some discussion of the model can be found in Ref. 3.

In order to decouple the statistics, the smallest cluster that has a bearing on the local correlation in the tetrahedral structure is a 16-bond cluster ($M=N/4$). The cluster unit of this example, shown in Fig. 1, includes a *C* spectator at the center, the four *A* or *B* alloy atoms surrounding it, and the twelve bonds to the *C* second neighbors. This 16-bond cluster has four alloy atoms (as does the classical tetrahedron of four atoms) but none of the alloy atoms is shared with neighboring clusters; the cluster is therefore four times larger than the simple tetrahedron. The cluster also shares no alloy atom pairs with neighboring clusters; indeed, the alloy atoms them-

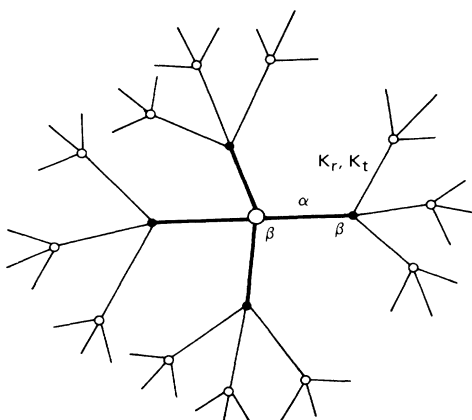


FIG. 1. Cluster unit used in Secs. III and IV. It includes a central *C* atom, the four neighboring *A* and *B* alloy atoms, and the 12 second neighbors to the central atom (shared with other clusters).

selves are not shared between clusters, and therefore the quasichemical statistics are exact. The only error lies in the approximation to the Hamiltonian, which must be constructed to make the cluster energy independent of the environment.

A. Strain energy

We begin by calculating the strain contributions to the cluster energies from a Keating force constant model.²⁰ To this are added the chemical terms³ for the total energy. Displacement of an atom from its equilibrium position gives rise to strain energies, given by

$$E_{\text{strain}} = \frac{3}{8d^2} \left[\alpha \sum_i \delta^2 \mathbf{r}_i \cdot \mathbf{r}_i + \beta \sum_i \sum_{j(j < i)} \delta^2 \mathbf{r}_i \times \mathbf{r}_j \right], \quad (26)$$

where δ^2 signifies the square of the difference in the dot or cross product relative to the unstrained value. The α terms are two-body radial forces (due to changes in equilibrium bond length) and the β terms are the weaker three-body (angular) forces. Typically, β is 5–10 times smaller than α . In the simplest approximation, every atom is constrained to sit at its average (virtual crystal) lattice site, and the strain energy arising from the difference in bond lengths of the respective pure *AC* and *BC* materials relative to the virtual crystal can be evaluated from Eq. (26). The strain energy so calculated severely overestimates the true strain energy because nuclei can displace from their virtual crystal positions to minimize the energy. A better approximation is to minimize the strain energy with respect to the possible distortions internal to the microcluster. If the twelve *C* atoms at the periphery of the cluster were constrained to sit at their virtual crystal positions, the Keating Hamiltonian, Eq. (26), for each cluster would be essentially uncoupled from its environment. Because the cluster approximation requires that the energy be uncoupled, such an approximation is appealing. With such a stiff lattice constraint, however, the strain energy calculated from Eq. (25) would still be overestimated, as Appendix A discusses. To approximate a more relaxed environment, we attach the 16-bond cluster to a fixed third shell. The bonds connecting the cluster and the fixed shell assume only the α force constant and $\beta=0$.

If one assumes that the force constants α and β are the same for all the bonds and that there are effective forces connecting the periphery *C* atoms outward, then it is possible to obtain an analytic expression for the strain energy, as shown in Appendix A.

B. Chemical energies

In an earlier paper³ we demonstrated that the energy minimization procedure that yields the equilibrium lattice spacings in alloys is affected only in second order by the small "chemical interaction" shifts. These chemical interactions are caused by differences between the atomic potentials and bond lengths of the constituents, and are coupled through the terms Harrison named *metallization*. Consequently, the bond lengths can first be determined by

minimizing energy configurations, as described above. Once these alloy bond lengths are found, they can be used to calculate the chemical excess energies. It has been shown that the excess energy associated with bond number 1 caused by a neighboring bond number 2 of a different chemical nature is given by

$$\Delta \epsilon_{cm} = f \Delta d + g \Delta V_3 + h (\Delta d)^2 + w \Delta d \Delta V_3 + u (\Delta V_3)^2, \quad (27)$$

where $\Delta d = d_2 - d_1$, $\Delta V_3 = V_3(2) - V_3(1)$, and the coefficients f , g , h , w , and u are various first and second partial derivatives of the metallization energies with respect to d and V_3 . Details and numerical values for all semiconductors can be found in Ref. 3. The only chemical excess energies included in the present calculation are those among the four bonds that join at the central C atom.

C. Numerical results

The microcluster excess energies were calculated by adding the strain energy in the Keating model (Sec. III A) to the chemical energy (Sec. III B). The force constants α and β were assigned their respective AC and BC pure crystal values. Energies were minimized to find the equilibrium local bond lengths.

The microcluster excess energies per 16-bond unit cell Δ_j from Eq. (19) are given as a function of composition for the alloy $\text{Ga}_{1-x}\text{In}_x\text{As}$ in Fig. 2. The major contribution to these excess energies stem from strains. For a given composition x , the clusters that fit most closely into the average lattice have the lowest energy. Thus,

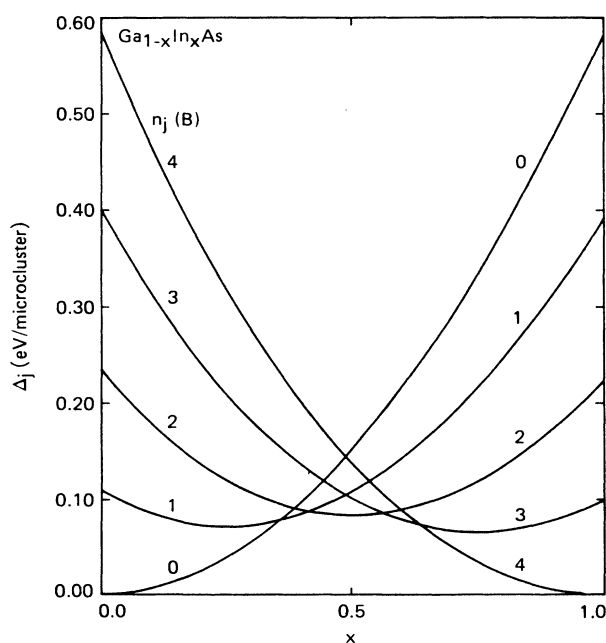


FIG. 2. $\text{Ga}_{1-x}\text{In}_x\text{As}$ alloy 5-atom, 16-bond cluster excess energy Δ_j , as a function of the alloy concentration x for clusters with differing numbers of In atoms, $n_j(B)=0,1,2,3,4$.

for example, at $x=0.5$, the $n_j(B)=2$ cluster has the lowest energy, while at $x=0$, the $n_j(B)=0$ cluster fits best. The nonequivalence of these curves arises from difference in force constants for GaAs and InAs. The average population deviations $\bar{x}_j - x_j^0$ from a random alloy calculated from Eq. (18) are given in Fig. 3 for growth temperatures of 600 and 1500 K. Notice that

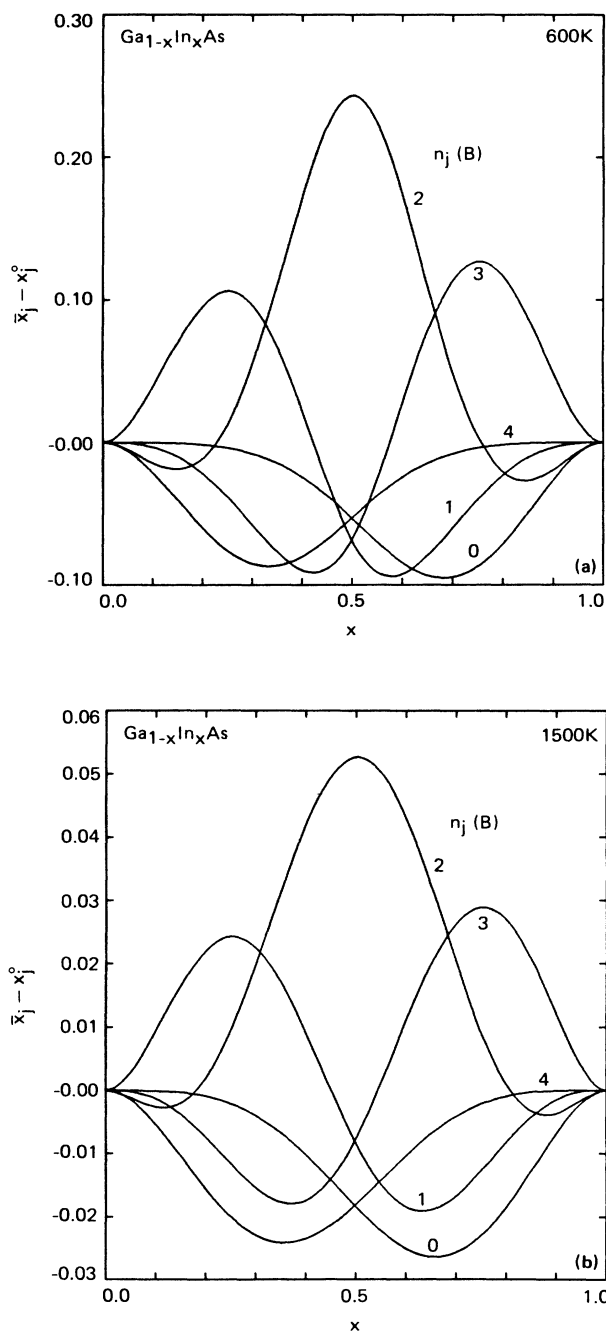


FIG. 3. $\text{Ga}_{1-x}\text{In}_x\text{As}$ alloy average cluster population \bar{x}_j . Average deviations, $\bar{x}_j - x_j$, from those of a random alloy x_j^0 as a function of concentration x for clusters with differing numbers of In atoms $n_j(B)=0,1,2,3,4, \dots$ and material grown at (a) $T=300$ K, or (b) $T=1500$ K.

the shapes of the curves at the two temperatures are similar, but the amplitudes of the deviation from random populations are much larger for the lower temperature. Moreover, some compositions show interchanges among the preferred populations at the different temperatures. Deviations from random populations are substantial. For example, at $T=600$ K and $x=0.5$, instead of the random population x_j^0 , 7,25,37,25,7 % for $j=0,1,2,3,4$, the values of \bar{x}_j are 2,18,60,18,2 %.

The mixing enthalpy (or average microcluster energy) per cluster (16 bonds), the mixing free energy per unit cell (four bonds), and the chemical potential μ'_B per microcluster are presented as a function of concentration x for four growth temperatures 300, 600, 1000, and 1500 K in Figs. 4(a), 5, and 6, respectively. The change in the shape of the mixing enthalpy ΔE versus composition x curves in Fig. 4(a) at different temperatures is quite small in this, our most realistic, model. The excess free energy variation in Fig. 5(a) is that expected for a material that exhibits an order-disorder transition with normal spinodal decomposition into domains of random alloys. However, the stiff surrounding lattice case (see Appendix C) in which the neighbors to the five-atom clusters are all held rigidly at their Vegard-rule lattice positions has also been evaluated in two cases. In the first case, the radial and bond angle restoring elastic constants α and β are set equal to their experimental values; in the second case, α retains its experimental value but β is set to zero. In the first case, strain energies are too large because the cluster volume is too highly constrained. In the second case, because there is no penalty for bond angle distortions, the clusters relax to lower energy configurations.

Differences between the models are qualitative as well as quantitative. The shapes of the ΔE and ΔF versus x curves in the realistic case and the two stiff-surroundings cases are dramatically different, as can be seen from Figs. 4 and 5. The sharp minima in ΔE in the curves in Fig. 4(c) and their smoothed-out corresponding features in ΔF in Fig. 5(c) at compositions $x=0.25, 0.5, 0.75$ (where periodic stoichiometric compounds are possible), are evident for these hypothetical materials prepared at low temperature. These materials would exhibit spinodal decomposition into domains of ordered compounds and random alloys, thereby predicting entirely different physical phenomena from those of Fig. 4(a) and 5(a). Our view of the proper physics will be reserved to the time when more results have been placed in evidence.

For completeness, the modified excess energy Δ'_j Eq. (20) for the various clusters is given in Fig. 7. From this figure, it is evident that the curvatures (nearly parabolas) for all the ϵ_j are related. In this version of the theory, most of the strain-energy information is carried in the chemical potential μ'_B .

The variations of the GaAs and InAs bond lengths in the different microclusters are shown in Fig. 8, and the concentrated weighted average values of these bond lengths—along with their root mean square (rms) deviations for alloys grown at 600 K—are given in Fig. 9(a). We have generated similar curves for alloys grown at 1500 K: they have a slightly smaller rms deviation than in the 600 K case and a bit smoother average transition

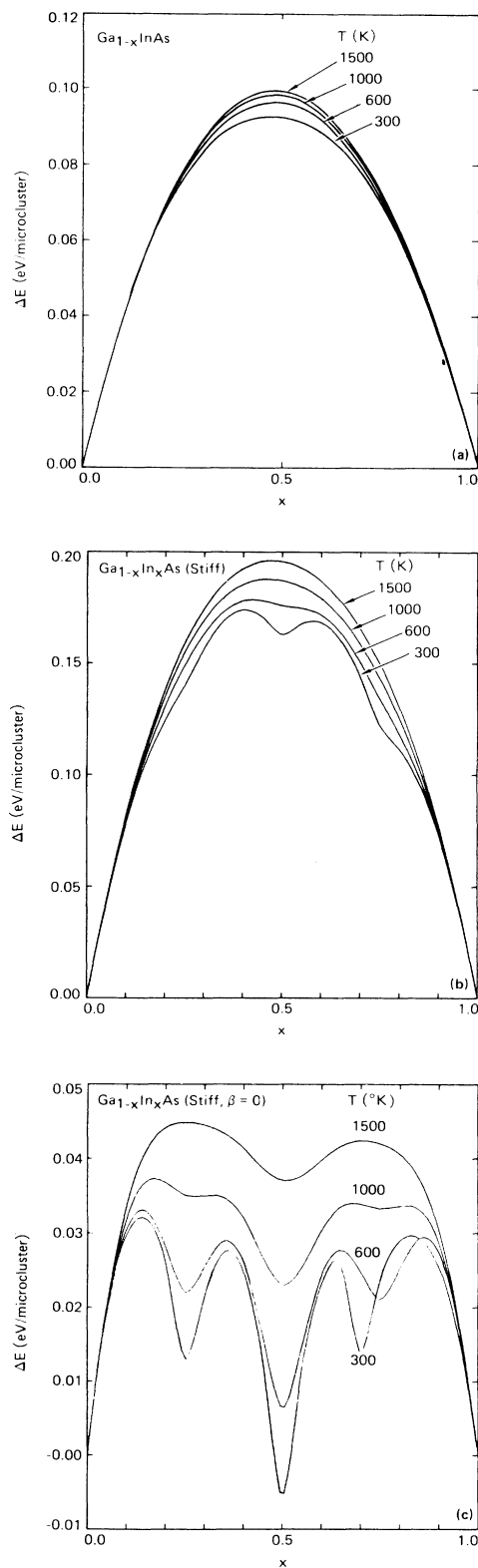


FIG. 4. $\text{Ga}_{1-x}\text{In}_x\text{As}$ alloy. Total excess energy ΔE in units of eV/microcluster (16 bonds) as a function of composition x for four different effective growth temperatures: 300, 600, 1000, and 1500 K. (a) The realistic soft model, (b) the stiff lattice model with realistic β , and (c) the stiff lattice model with $\beta=0$.

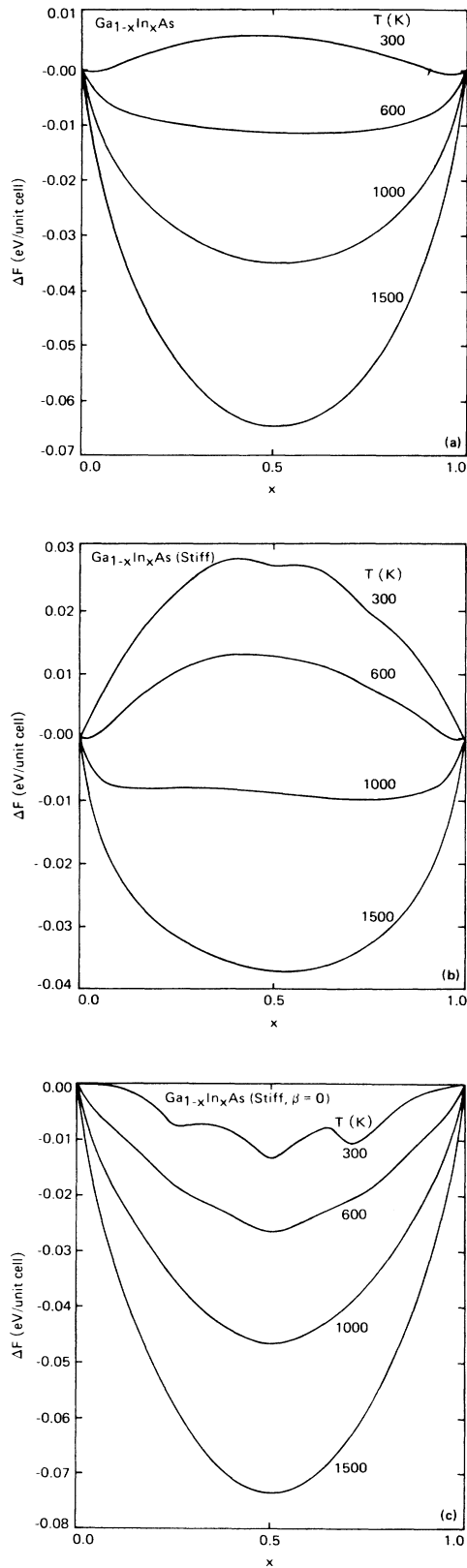


FIG. 5. $\text{Ga}_{1-x}\text{In}_x\text{As}$ alloy excess free energy in units of eV/unit cell (four bonds) as a function of concentration x for the four growth temperatures and cases identified in Fig. 4.

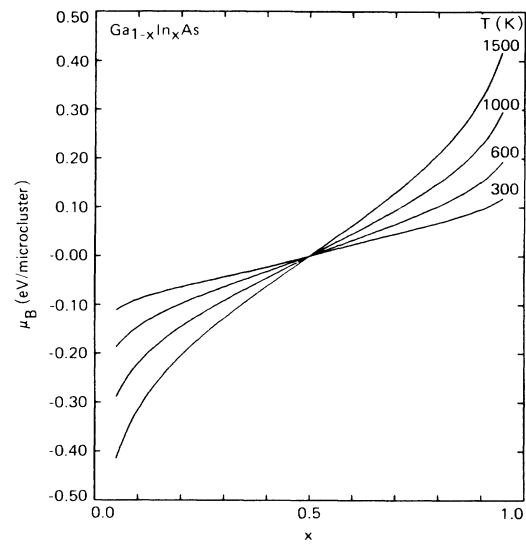


FIG. 6. $\text{Ga}_{1-x}\text{In}_x\text{As}$ alloy In atom chemical potential μ_B in units of eV/microcluster as a function of concentration x for four effective growth temperatures: 300, 600, 1000, and 1500 K.

from $x=0$ to 1, but the differences between the two cases are small. These curves fit the extended x-ray-absorption fine-structure (EXAFS) data of Mikkelsen and Boyce²¹ quite well. For comparison, in Figs. 9(b) and 9(c) the \bar{d} curves are also presented in the two stiff-surrounding cases. All these curves exhibit the same trends although the stiff cases have less relaxation, larger rms deviations, and larger deviations from the EXAFS results.

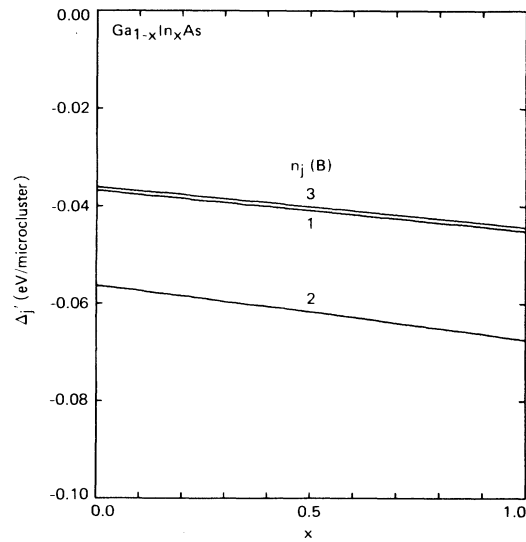


FIG. 7. $\text{Ga}_{1-x}\text{In}_x\text{As}$ alloy reduced microcluster excess energy Δ_j' in units of eV/microcluster as a function of composition x with differing numbers of In atoms $n_j(B)=1,2,3$; $\Delta'_0=\Delta'_4=0$ by definition.

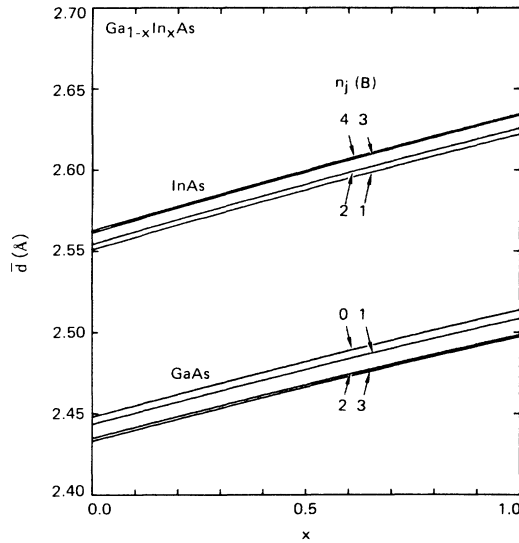


FIG. 8. $\text{Ga}_{1-x}\text{In}_x\text{As}$ bond lengths for InAs and GaAs bonds in 5-atom clusters with differing numbers of In atoms $n_j(B)=0,1,2,3,4$ as a function of concentration x .

For comparison, an anion-substituted alloy $\text{GaAs}_{1-x}\text{Sb}_x$ with a lattice mismatch of 7.8% similar to that of $\text{Ga}_{1-x}\text{In}_x\text{As}$ 7.1% was treated. Figures 10–13 are the equivalent ones to compare with Figs. 4, 5, 8, and 9. This result runs counter to the general trend between the cation- and anion-substituted alloys, pointed out previously.³ The chemical terms smooth the curves in the cation-substituted case (decrease mixing enthalpy parameters, decrease critical order-disorder temperatures) but enhance the rough features of the curves in the anion-substituted case. The difference is easily discerned by comparing the excess enthalpy curves in Figs. 4(a) and 10. Despite the fact that the lattice mismatch is larger in $\text{GaAs}_{1-x}\text{Sb}_x$ than in $\text{Ga}_{1-x}\text{In}_x\text{As}$, the curves in Fig. 10 have a smaller temperature variation than those in Fig. 4(a). Both sets of curves have comparable energy magnitudes but, as one would expect, the $\text{GaAs}_{1-x}\text{Sb}_x$ values are slightly larger. Once again the ΔF , d , and \bar{d} variations are as expected.

In Table I the mixing enthalpy parameter Ω is collected for several alloys. It is traditional to extract the temperature-independent part of ΔF and identify it with the enthalpy ΔE , then to fit ΔE to the functional form $\Delta E = x(1-x)\Omega$. Judging from the present theory (see Fig. 4), this procedure is clearly flawed, so that comparisons among the results in Table I should be made with caution. However, it is clear that the more realistic soft-lattice model, in which the surroundings are permitted to accommodate to the local cluster, yields numbers that are closer to the experimental results than does the stiff model, where the theoretical numbers are generally factors of 2 to 3 larger than the experimental results. The nearly bond-length-matched alloys such as $\text{Ga}_{1-x}\text{Al}_x\text{As}$ and $\text{Hg}_{1-x}\text{Cd}_x\text{Te}$ are exceptions. For them, the electron-electron interactions, neglected in the theory leading to

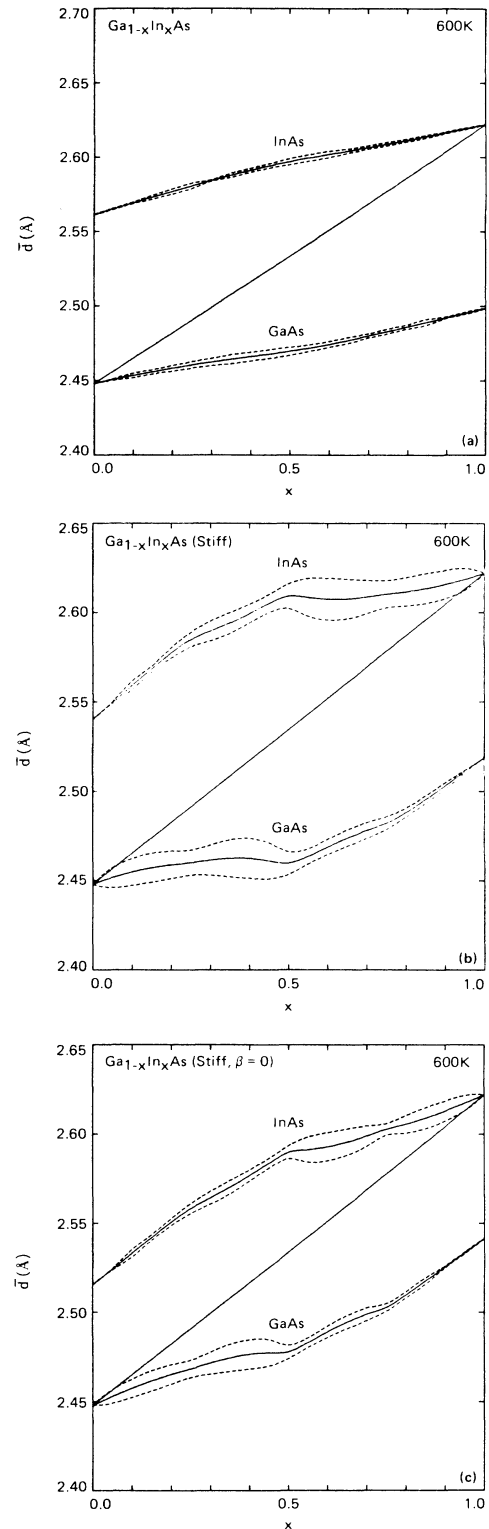


FIG. 9. $\text{Ga}_{1-x}\text{In}_x\text{As}$ alloy average GaAs and InAs bond lengths as a function of composition x for material grown at 600 K. The solid curves labeled GaAs and InAs are the average values, and the dashed curves are the extent of the rms variations. The heavy solid line is the average bond length corresponding to Vegard's rule in the three models (a), (b), and (c) identified in Fig. 4.

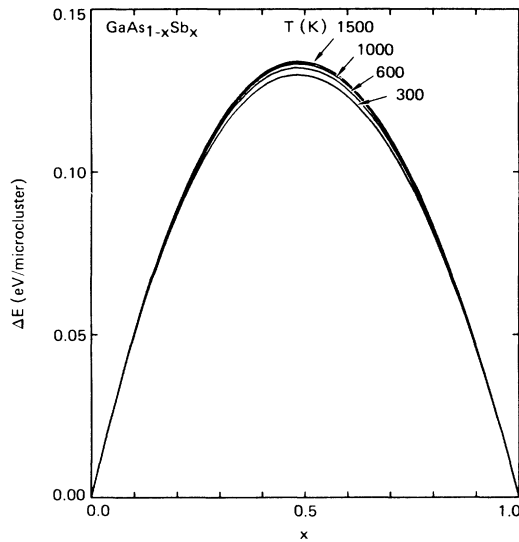


FIG. 10. $\text{GaAs}_{1-x}\text{Sb}_x$ alloy total excess energy ΔE in units of eV/microcluster (16 bonds) as a function of concentration x for four different effective growth temperatures: 300, 600, 1000, and 1500 K.

the results in Table I, are responsible for the observed mixing properties.⁴

IV. CONCLUDING REMARKS

We have demonstrated^{2-4,22} that the atomic distribution of constituents in semiconductor alloys is never truly

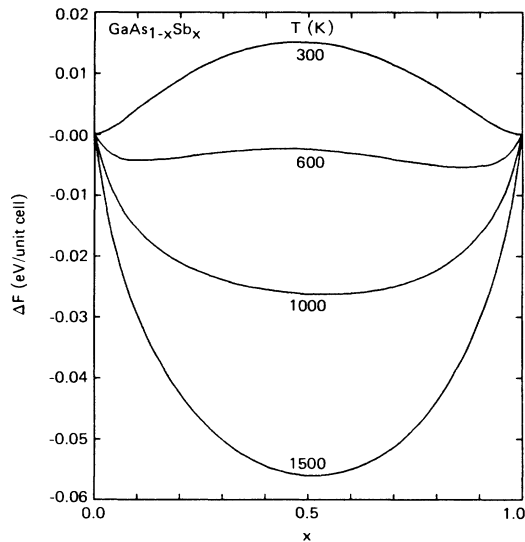


FIG. 11. $\text{GaAs}_{1-x}\text{Sb}_x$ alloy excess free energy ΔF in units of eV/unit cell (4 bonds) as a function of concentration x for the same temperatures as in Fig. 10.

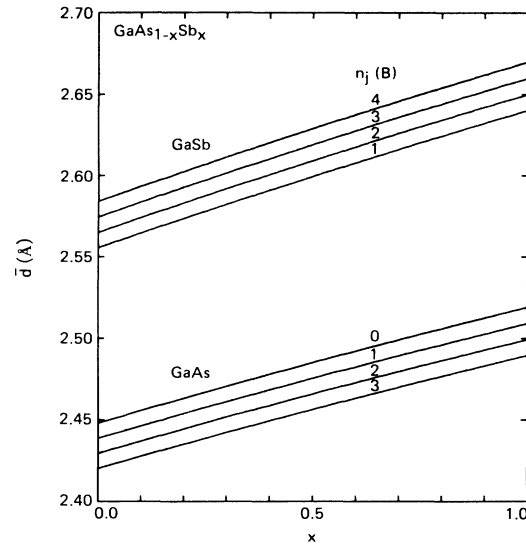


FIG. 12. $\text{GaAs}_{1-x}\text{Sb}_x$ bond lengths for GaAs and GaSb bond in 5-atom clusters with differing numbers of In atoms $n_i(B)=0,1,2,3,4$ as a function of concentration x .

random. There are always interactions causing correlations; the degree and nature of the correlations depend on which interactions dominate and on the growth conditions. While we have identified most of the interactions expected to cause correlations, not all of them have been treated completely in this paper. However, even though some details remain unclear, the principal effects can now

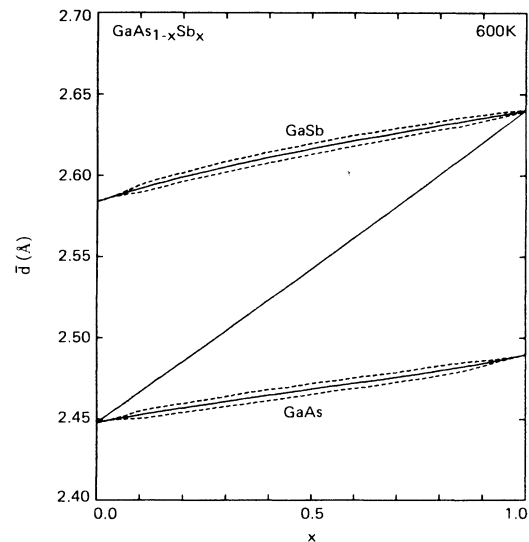


FIG. 13. $\text{GaAs}_{1-x}\text{Sb}_x$ alloy average GaAs and GaSb bond lengths as a function of composition x for material grown at 600 K. The solid curves labeled GaAs and GaSb are the average values, and the dashed curves are the extent of the rms variations. The heavy solid curve is the average bond length corresponding to Vegard's rule.

TABLE I. Mixing enthalpy parameter Ω in units of kcal/mol, calculated at $T=1000$ K with the "soft" and "stiff" models. For comparison, results are included from Ref. 3 from the full perturbation theory (FPT) and experimental numbers (Expt).

	Soft	Stiff	FPT	Expt.
CdHgTe	0.033	0.038	-0.07	0.7,1.4
ZnHgTe	1.552	2.613	1.50	3.0
CdZnTe	1.592	2.718	1.24	1.34
AlGaP	0.013	0.026	-0.05	
GaInP	2.854	5.454	2.54	3.25,3.5
AlInP	2.662	4.775	2.55	
AlGaAs	0.027	0.044	-0.07	0.0
GaInAs	2.178	4.328	1.60	1.65,2.0,3.0
AlInAs	2.257	4.319	2.17	2.5
AlGaSb	0.116	0.179	-0.15	0.0
GaInSb	1.715	3.266	0.81	1.47,1.9
AlInSb	1.459	2.833	1.36	0.60
ZnSSe	0.945	1.700	0.90	
ZnSeTe	2.156	3.713	2.26	1.55
ZnSTe	6.115	9.338	6.20	
AlPaS	0.666	1.364	0.76	
AlAsSb	3.447	6.477	4.09	
AlPSb	6.935	12.019	8.32	
GaPAs	0.741	1.589	0.94	0.4,1.0
GaAsSb	2.922	5.797	3.67	4.0,4.5
GaPSb	6.556	12.473	8.66	
InPAs	0.519	1.035	0.57	0.4
InAsSb	2.199	3.989	2.52	2.25,2.9
InPSb	4.969	8.325	5.76	

be appreciated in broad terms; we attempt to identify them in the following.

In the formalism reported here, we start by focusing on small clusters of atoms that are called *microclusters*. Once the microcluster size is selected, the total energy of the solid is expressed as a sum of cluster energies, and the number of configurations of the solid corresponding to a given total energy is calculated. There are approximations in the microcluster energy calculations and microcluster-microcluster interactions are neglected, but once these approximations are made, no appreciable additional inaccuracy is introduced in the statistical mechanics arguments leading to microcluster population distributions. The accuracy of the final result for a given physical property (e.g., critical order/disorder transition temperature) differs for different properties, but in general becomes progressively better the larger the cluster size used. Two-atom clusters are found to give most trends properly, but differ in detail from the answers found for the 5-atom, 16-bond clusters that are the basis for most of the numerical results in this paper. We have not attempted to extend the numerical results to large clusters because larger clusters will not help in the understanding of the long-range corrections, and the present cluster is adequate to describe the most important local correlations.

An n -atom microcluster in state j , represented schematically as $A_{n-n_j(B)}B_{n_j(B)}$, corresponds to a given number $n_j(B)$ of B atoms. If the degeneracy $g_j = \binom{n}{n_j(B)}$ of a given energy state ϵ_j is not split, and if ϵ_j depends linearly on $n_j(B)$, the average population distribution of such a mi-

crocluster, \bar{x}_j , is always that of a random alloy x_j^0 . Therefore, only interactions that split the degeneracy or cause a nonlinear variation of ϵ_j on $n_j(B)$ drive correlations. To be precise (as detailed analysis shows), the energies $\epsilon_j - n_j(B)\mu(B)$, where $\mu(B)$ is the B atom chemical potential in the grand partition function formalism, are responsible for populations of state j .

Three mechanisms cause appropriate nonlinear variations of ϵ_j . A type caused by strains resulting from bond-length mismatches between the constituents. So-called *chemical interactions*, caused by potential differences between the constituents that are responsible for charge shifts among the atoms, and in tight-binding terminology the ionic, covalent, and metallization contributions to bond energies. A type arising from the electron/electron Coulomb interactions as modified by long-ranged Madelung sums.⁴ As a rule, the bond-length mismatch terms dominate, but the other term can introduce substantial corrections and are all that remain in cases where there is a near-bond-length match. Until recently, it was thought that cluster energies were nearly independent of composition.⁷ In consequence, if the average of the AA and BB interaction energies exceeded the AB energy, then compound formation was thought to be favored while an AB energy exceeding the interaction energies was thought to favor spinodal decomposition. The entropy terms would always favor the intermediate random distribution.

We now know that this picture is flawed and that the cluster excess energies are in fact highly composition

dependent. In the strain terms, the cluster whose volume most closely matches the average volume per cluster for the alloy will have the lowest energy. As a consequence, certain alloy compositions (e.g., $x=0.25, 0.5, 0.75$, where simple stoichiometric compounds with long-range order could exist) have comparatively low excess-free energies. This means that it is possible in principal to have a positive mixing enthalpy parameter defined by $\Omega \equiv \Delta E / [x(1-x)]$ and still have compound formation favored for some special composition's x . However, this does not happen as a general rule. For example, in Fig. 4(a) the excess enthalpy ΔE has no sharp feature at the special concentrations, even for material grown at room temperature. The shape of the corresponding free energy ΔF in Fig. 5(b) is characteristic of a material that undergoes normal spinodal decomposition. Figure 5(b) displays the excess free energies ΔF for a stiff-lattice case of $\text{Ga}_{1-x}\text{In}_x\text{As}$, in which it has been assumed that the 12 outer bonds of the cluster are attached to C-type atoms that are fixed at lattice spacings corresponding to Vegard's rule. Even in this stiff-lattice case, normal spinodal decomposition is the rule. It is not until we also set the angular distortion elastic constant β in the valence force field model to zero that the excess free energy curve for $\text{Ga}_{1-x}\text{In}_x\text{As}$ in Fig. 5(c) has a shape that corresponds to decomposition into an ordered compound and a random alloy. We have resisted the temptation to present phase diagrams (critical temperature versus composition) in this paper because they will be modified by the electron-electron Coulomb interactions that are not yet incorporated completely into the formalism.

The chemical interactions modify this picture only slightly: They tend to cause a slight asymmetry in the excess enthalpy variation with x about $x=0.5$ and to shift the overall curves. For $\text{Ga}_{1-x}\text{In}_x\text{As}$, the asymmetry causes the features on the low- x side to have higher energies than the corresponding ones on the high- x side. Despite the fact that the bond-length mismatch is slightly greater for $\text{GaAs}_{1-x}\text{Sb}_x$ than for $\text{Ga}_{1-x}\text{In}_x\text{As}$, causing ΔE to be larger, the temperature variation of ΔE is actually smaller for $\text{GaAs}_{1-x}\text{Sb}_x$. This runs counter to conclusions we drew previously,³ based on single impurity considerations where chemical excess energies tended to be positive for anion-substituted alloys and negative for cation-substituted alloys.

The configuration-dependent electron-electron Coulomb interactions⁴ are not included in the results reported here. These interactions make contributions comparable to those driven by the bond-length differences discussed previously and, therefore, will modify the numerical results significantly. The terms are driven by polarity differences between the alloy constituents in contradistinction to the customary bond-length difference. The essential feature of Coulomb interactions is the configuration-dependence of spatial charge fluctuations. Because the Coulomb energy is nonlinear in the charge density, fluctuations increase the energy. This can be partially compensated by the long-range Madelung energy originating in a coherent sum of alternating charges. Configurations that minimize the combined effect are of lowest energy. The random configuration is always of

higher energy, mainly because of the weakening of the Madelung energy. Therefore, both ordered compounds and spinodal decomposition are favored by this interaction relative to random alloys. We have demonstrated that in the bond-length-matched $\text{Ga}_{1-x}\text{Al}_x\text{As}$ alloy, the ordering observed by Kuan *et al.*²³ can be explained by electron-electron Coulomb terms.

Others^{8-10,12} have calculated the concentration variation of microcluster energies ε_j by treating the various types of clusters as units of different periodic structures. Several of these workers allow the central atom in each $A_{4-j}B_jC$ ($j=0,1,2,3,4$) microcluster to relax into its minimum-energy configuration and then compute the energy of the cluster $\varepsilon_j(v)$ as a function of cluster volume v . They then assign cluster energies at each composition x by identifying the v to be that of the average lattice, following Vegard's rule. Because of long-range effects, this procedure leads to small, sometimes negative, excess cluster energies, Δ_j for the compositions where the cluster volume just fits the average alloy volume per cluster, so these special clusters experience no strain. Moreover, coherent band effects also tend to lower the energy. In the plot of Δ_j versus x in Fig. 2, this would cause the $A(3)B(1)C$, $A(2)B(2)C$, $A(1)B(3)C$ cluster energies to be small for $x=0.25, 0.5$, and 0.75 , respectively. In addition, the constraint that each type of cluster has the same volume at a given concentration accentuates the differences between cluster energies relative to those we calculate and produces Δ_j curves that resemble the stiff lattice case. The energies are then scaled upward by two groups^{8,9} to cause the mixing enthalpy to have the correct value. It is argued that these extra terms are needed in one case to account for the fact that the band-structure theory leads to bond-length differences that are too small,⁹ and in the other because the angular restoring forces were set to zero.⁸

In our procedure each cluster is attached to an effective alloy medium and allowed to relax to its minimum-energy configuration. The effect of constraining the volume can be seen by comparing Figs. 4(a) and 4(b). Thus there are two major differences between our ε_j versus x curves and those of other groups. Even for cases with a bond-length mismatch, some of their Δ_j values are negative for a collection of special concentrations corresponding to possible stoichiometric compounds for which the periodic lattice can fit together without appreciable strain. Furthermore, their Δ_j values vary much more steeply with x reaching somewhat larger values and having a much larger overall excursion, because the various cluster volumes are each forced to equal the average lattice volume. This causes their excess enthalpy and free energy versus composition curves at a given temperature to have a much sharper structure than ours with three minima at $x=0.25, 0.5$, and 0.75 . To generate the similar results shown in Figs. 4(c) and 5(c), we had to adapt the unphysical approximation of setting the angle-restoring elastic coefficient β to an unrealistically small value.

There is merit in the approaches taken in Ref. 9 when an alloy has long-range order; their energies are then more appropriate (but one should not use cluster statistics). The models reported to date assign to a microclus-

ter only the local strain energy. However, a long-range strain field is also produced in the surrounding medium by a cluster that does not fit exactly into the lattice. If there are many misfitting clusters, then the long-range strain fields from each add incoherently, and the net result is to produce the average lattice spacing, but no additional nonlocal energy need to be counted toward each cluster. We depend on this in our cluster-energy calculation; it is the reason long-range strain fields are not included in the cluster energies. However, when the misfit cluster density is small, then the incoherence is incomplete and the long-range strain fields are likely to be important. Thus starting from a perfectly ordered compound, e.g., ABC_2 , the first small deviation in the composition from the ideal stoichiometry will introduce large (local and long-range) strain fields, which will cause the composition variation of the free energy around these special points to be even more rapid than anyone has yet calculated. Accordingly, the net result is expected to be low-temperature excess-free-energy curves that resemble those in Fig. 5(a), but with sharp negative spikes superimposed at the special compositions. This conjecture remains to be confirmed by calculation and experiment.

The other major class of phenomena that can introduce correlations is made up of phenomena that split the degeneracy of the clusters. The easiest to picture are coherent strains produced by a uniform externally applied stress as, for example, when an epitaxial layer of an alloy is grown on a lattice-mismatched substrate. Then, for example, for a stress in the $\langle 110 \rangle$ direction, a four-atom $n_j(B)=2$ cluster will have different energies if the two B atoms or two A atoms have positive displacement components parallel to the $\langle 110 \rangle$ direction. When the stress is large enough to drive the energy of the preferred orientation down well below those of other clusters, then it is possible for compounds with long-range order to have low free energies. This phenomenon has recently been observed in the growth of $Ge_{0.5}Si_{0.5}$ on a silicon substrate, where an ordered compound, rather than a random alloy, was found.¹⁴ Stresses produced by temperature gradients behind a growth front can cause similar effects. In this discussion we have recognized the potential importance of applied stresses and temperature gradients in driving microcluster population distributions. While a special case has been treated,²⁴ a comprehensive quantitative theory must still be formulated.

We have discussed the possibility of spinodal decomposition into domains. A given domain can be nearly a random alloy surrounded by other domains with differing compositions or ordered compounds depending on the constituent materials, the concentration, and growth conditions. However, there remains the question of how the domains fit together and their relative size. We cannot offer complete answers to these questions, but we can identify many phenomena that influence the outcome. The thermodynamics discussed here tell us about the compositions and structure of the favored domains. Clearly, if there is no inhibition to atom motion or annealing times are sufficiently long for equilibrium to be reached, the system will separate into two domains, one of each of the favored types, and the relative amount of each

type will be given by the composition-lever rule applied to the free-energy curve. However, if there are constraints on the distance atoms can travel, then other local-free-energy minima may be determined by a competition between the statistical effects discussed previously and long-range strains produced as the alloy forms a domain structure. Because the different types of domains have different lattice constants when they fill space in some regular array, they will exert stresses on one another. The preferred configuration will be one that minimizes the net free energy, now including the extra mechanical domain-domain interactions. The calculation by Muller,¹⁵ in which he demonstrates that the fluctuations in the populations of clusters inherent in a random alloy are suppressed by strain fields in lattice-mismatched systems, is a precursor to this kind of theory. A regular array of domains of ordered compounds surrounded by a random alloy has been reported recently by Jen, Cherng, and Stringfellow.²⁵

A number of nonequilibrium growth processes are proving to be valuable additions to our materials preparation methods. Included in this category are all growth methods in which the substrate is held at a temperature well below the melting point of the growing material, e.g., molecular beam epitaxy (MBE), metalorganic-chemical-vapor deposition (MOCVD), and various energy-assisted epitaxies (EAE).^{26,27} The EAE methods are those in which some form of energy, e.g., laser light or ion bombardment, is supplied to the growing surface. Even without energy assistance, local bonding arrangements in the layers just beneath the growth surface can reorder to attain local-minimum-free-energy configurations driven by the energy released when the new atoms arrive and bond, typically a few eV per atom. If one thinks in terms of an effective growth surface temperature, T_{eff} , that determines the nature of the order/disorder phase state of the material, then in normal MBE and MOCVD, T_{eff} probably lies below the melting temperature T_m . For liquid-phase epitaxy, one has $T_{\text{eff}} \approx T_m$, while for EAE, one has $T_{\text{eff}} > T_m$. This single T_{eff} parameter model is undoubtedly an oversimplification, but it serves to establish an order among the trends of a wide range of experimental results recently reported. When T_{eff} is small (MBE and MOCVD), then correlations are high, and ordered crystals and crystals with ordered arrays of domains can occur. When $T_{\text{eff}} \approx T_m$, then correlations are smaller and, depending on the alloy and composition, more nearly random arrangements or normal spinodal decomposition are more likely. When $T_{\text{eff}} \gg T_m$, then it is possible to grow materials in the form of random alloys that do not exist in equilibrium. While these materials are metastable, they may still be useful and open a whole new treasure trove to device science.

ACKNOWLEDGMENTS

This work was supported in part by U.S. Air Force Office of Scientific Research Contract No. F49620-85-C0023 and U.S. Office of Naval Research Contract No. N00014-85-K-0448.

APPENDIX A: ANALYTICAL EXPRESSIONS FOR THE CLUSTER STRAIN ENERGY

We can sidestep the complication of the way to couple the cluster to its environment for the present by modifying the Keating model for the bonds to the C atoms at the periphery. The force constant model in Eq. (26) is used for the bonds connecting the central atom to its four neighbors and also includes the 12 three-body β forces connecting the central atom to the 12 peripheral C atoms. The 12 bonds to the peripheral atoms are coupled by effective force constants K_r and K_t , which characterize the resistance of displacement of the alloy atom transverse and normal to the bond. This entails no further approximation (beyond assuming that the K 's do not couple to each other through bonds outside the cluster), since it is possible to obtain K_r and K_t in terms of α and β . However, the dependence of the K 's on α and β requires some detailed model that governs the displacement of the 12 peripheral C atoms and their effective interaction with the more remote bonds. By using K_r and K_t , we can leave this choice and also the displacement of the peripheral atoms unspecified.²⁸ K_r and K_t are evaluated for a particular model in Appendix B.

The total strain energy is thus formulated as the sum of strain energies internal to the microcluster, which we calculate from the Keating model, the three-body β strain energies connecting the microcluster to the adjacent effective medium atoms, and the strain energy from the effective medium,

$$\frac{1}{2}K_r \sum_{i,j} (\hat{d}_{ij} \cdot \delta \mathbf{r}_j)^2 + \frac{1}{2}K_t \sum_{i,j} |\hat{d}_{ij} \times \delta \mathbf{r}_j|^2, \quad (\text{A1})$$

where the index i signifies each of the three external bonds adjacent to microcluster atom j , and $\delta \mathbf{r}_j$ represents the displacement of a nucleus relative to its natural bond position.

The resulting strain energies for the A_4 and B_4 microclusters can be expressed in terms of the differences δ_A and δ_B in bond lengths of the pure crystals A and B relative to that of the virtual crystal bond length d , defined as

$$\delta_A \equiv d - d_A, \quad (\text{A2})$$

and

$$\delta_B \equiv d - d_B. \quad (\text{A3})$$

The strain energy of each cluster must be minimized with respect to the various possible independent distortions. By symmetry, the only distortion A_4 and B_4 microclusters can suffer is the breathing mode in which every A atom displaces radially by an equal amount. If we minimize with respect to the radial displacement, the strain contribution to the excess energy is

$$E_{A_4} = E_{4,\text{strain}} = C_B \delta_A^2, \quad (\text{A4})$$

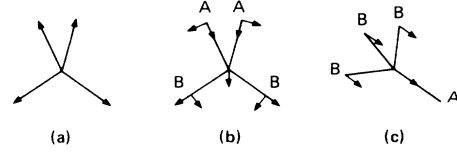


FIG. 14. Distortions of a tetrahedron (a) breathing mode distortion of A_4 and also in the other microclusters as described in the text. (b) Distortion in A_2B_2 corresponding to bond-length differences $d_A - d_B$. There are three independent distortions: a radial distortion along the bond axis, a distortion transverse to the bond axis, and the displacement of the central C atom. (c) Distortions in A_3B or AB_3 , corresponding to bond-length differences $d_A - d_B$. There are three independent distortions here as well: a uniform translation of all atoms in the microcluster (not shown), the displacement of the central atom, and the displacement of the three A (or B) atoms transverse to the bond axes.

and

$$E_{B_4} = E_{0,\text{strain}} = C_B \delta_B^2, \quad (\text{A5})$$

where the effective breathing-mode force constant C_B takes the form²⁹

$$C_B = \frac{96(64\alpha K_r + 27\alpha\beta + 32\alpha K_t + 16K_r\beta + 32K_r K_t)}{576\alpha + 64K_r + 243\beta + 512K_t}. \quad (\text{A6})$$

The A_2B_2 microcluster has five independent distortions, illustrated in Fig. 14. To minimize the internal energy, the simultaneous equations $\nabla_{u_j} E_{\text{strain}} = 0$ must be solved, where the u_j are coefficients each to some linear combination of the displacements shown in Fig. 14. The symmetric combinations of radial and transverse displacements of A and B atoms uncouple from the remaining three independent distortions. Thus there is a breathing mode (the symmetric radial displacement), a mode that vanishes identically at the undistorted lattice position, and finally a “displacive” mode. The strain energy is comprised of a sum of the first and last modes,

$$E_{A_2B_2} = E_{2,\text{strain}} = C_B \left[\frac{\delta_A + \delta_B}{2} \right]^2 + C_D \left[\frac{\delta_A - \delta_B}{2} \right]^2, \quad (\text{A7})$$

where C_D is the effective displacive mode force constant. Because C_D is numerically more complicated than C_B , we show the form C_D using $K_t = \beta$. It is²⁹

$$C_D = \frac{512\beta K_r [688\alpha K_r + 1807\alpha\beta + 212K_r\beta]}{3[512\alpha K_r^2 + 80\beta K_r(199\alpha + 8K_r) + 3677\beta^2(9\alpha + 2K_r)]}. \quad (\text{A8})$$

The A_3B and AB_3 microclusters have four independent distortions, but the same breathing mode and bending modes found in the A_2B_2 microcluster can be extracted with a suitable linear combination of atomic displacements. The energy then takes the form

$$E_{AB_3} = E_{1,\text{strain}} = C_B \left[\frac{\delta_A + 3\delta_B}{4} \right]^2 + \frac{3}{4} C_D \left[\frac{\delta_A - \delta_B}{2} \right]^2. \quad (\text{A9})$$

The cluster energies take a particularly simple form, depending only on x , C_B , and C_D . Figure 15 shows the dependence on α and β of C_B , C_D , and K_r as estimated in Appendix B. If the virtual crystal bond length is assumed to be linear in the composition x (as is nearly the case experimentally), the strain energies assume a simple quadratic dependence on x , all with the same curvature in this model. If the strain energies alone are considered, the free energy must be symmetric in $x - \frac{1}{2}$, in which case it must be true that $\mu_B(x) = -\mu_B(1-x)$, and $\mu_B(\frac{1}{2}) = 0$. For $x = \frac{1}{2}$ the partition function is

$$q = 2(3e^{-C_D(d_A - d_B)^2/4kT} + 4e^{-(3C_D + C_B)(d_A - d_B)^2/16kT} + e^{-C_B(d_A - d_B)^2/4kT}). \quad (\text{A10})$$

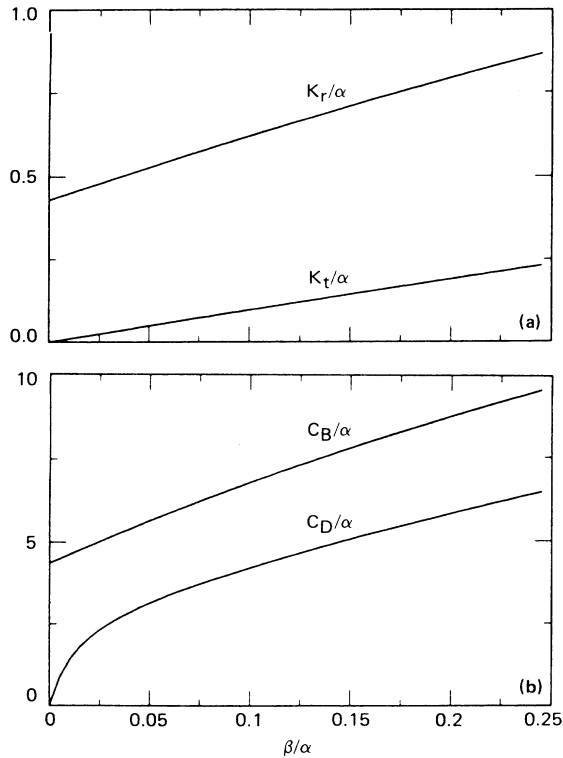


FIG. 15. Variation with β of K_r as estimated from Eq. (A8), K_t obtained from Eq. (A6), C_B and C_D using Eqs. (A6) and (A8) for K_r and K_t . All force constants are in units of α to make them dimensionless. Typically $\alpha/10 < \beta < \alpha/5$ (see Table I).

Given this partition function, all of the thermodynamic quantities of the system related to strain induced by lattice mismatch can be calculated. However, the numerical results reported in the body of this paper use a more exact relation. Equation (A10) provides useful insights into the underlying physics, but it is not used in our numerical evaluations.

APPENDIX B: EVALUATION OF FORCE CONSTANTS

For purposes of generating K_r and K_t , we treat the medium surrounding the cluster as a virtual crystal in which the cluster is embedded. The reason this is a proper choice to represent the average medium is subtle. The alloy is made of a collection of clusters with a distribution of sizes. If one places an atom or cluster in a medium that is, for example, too large, both it and the surroundings will be compressed, thereby establishing a long-range strain field in the surroundings. The net strain field is that due to the combined effect of all the clusters. But for a nearly random concentrated alloy, at any point in space the long-range contributions to the strain add incoherently and average to zero relative to the position corresponding to the virtual crystal lattice. Thus only the short-range local interactions contribute to the strain energies and are counted. In alloys with significant correlations, e.g., nearly ordered compounds, or in dilute alloys where the long-range strain fields do not average to zero, the problem is more complicated. The dilute limit is treated in detail in our prior work.³ As an exact solution of the Keating model includes long-range strain fields, approximations are necessary.⁹ K_r and K_t will depend on the approximation used to govern the displacement of the 12 peripheral C atoms and more distant neighbors, but it is generally true that the numerical values of K_r and K_t are rather similar for the various approximations one might consider. In particular, K_t is weak, and can be very well approximated by holding the distant atoms fixed, allowing the nearest C atom to move freely. In that approximation, K_t becomes

$$K_t = \beta[1 - (\beta/4\alpha)] \approx \beta. \quad (\text{B1})$$

(The latter approximation obtains if the C atom is also fixed.)

K_r is more sensitive to the assumptions governing the displacement of the virtual crystal atoms, and is necessarily more complicated. If, in the simplest assumption, the C atom is held fixed,

$$K_r = 3\alpha + \beta/4 \quad (\text{B2})$$

a value significantly too large, as the following shows. A reasonably good approximation is to take the third neighbors as fixed, and neglect the β forces coupling second and third neighbors (the Shih³⁰ approximation, but extended to the second neighbor shell). Then,¹⁴

$$K_r = \frac{3\alpha + 16\beta}{7[1 + (\beta/2\alpha)][1 + (\beta/14\alpha)]}, \quad (\text{B3})$$

which is roughly four times smaller than the rigid approximation Eq. (A7).

Because the total energy is rather sensitive to K_r , this

approximation (or a similar one) is probably the most important one of the model. The sensitivity of the total energy to K_r is most easily expressed as $\partial \ln C_B / \partial \ln K_r$. At $K_t = \beta$ and $K_r = \alpha$, both $\partial \ln C_B / \partial \ln K_r$ and $\partial \ln C_D / \partial \ln K_r$

are $\approx \frac{3}{4}$, while $\partial \ln C_B / \partial \ln K_t$ and $\partial \ln C_D / \partial \ln K_t$ are ≈ 0.025 . Thus the variation of the total energy is almost directly proportional to K_r , while it is only weakly dependent on K_t .

¹In a pseudobinary alloy, the A and B atoms occupy one crystalline sublattice and the C atoms another. The C atoms are merely spectators in the statistics.

²A.-B. Chen and A. Sher, *Mat. Res. Symp.* **46**, 137 (1985).

³A.-B. Chen and A. Sher, *Phys. Rev. B* **32**, 3695 (1985).

⁴M. van Schilfgaarde, A. B. Chen, and A. Sher, *Phys. Rev. Lett.* **57**, 1149 (1986).

⁵R. Kikuchi, *J. Phys. (Paris), Colloq.* **38**, C7-307 (1977).

⁶M. Kurata, R. Kikuchi, and T. Watari, *J. Chem. Phys.* **21**, 434 (1953).

⁷E. A. Guggenheim, *Mixtures* (Clarendon, Oxford, 1952).

⁸M. T. Czyzyk, M. Podgorny, A. Balzarotti, P. Lelardi, N. Motta, A. Kisiel, and M. Zemnal-Slarnawska, *Z. Phys. B* **62**, 153 (1986).

⁹G. P. Srivastava, J. L. Martins, and A. Zunger, *Phys. Rev. B* **31**, 2561 (1985).

¹⁰M. Ichimura and A. Sasaki, *J. Appl. Phys.* **60**, 3850 (1986).

¹¹R. Kikuchi, *Phys. Rev.* **81**, 988 (1951).

¹²A. A. Mbaye, L. G. Ferreira, and A. Zunger, *Phys. Rev. Lett.* **58**, 49 (1987).

¹³E. Schrodinger, *Statistical Thermodynamics* (Cambridge University Press, Cambridge, 1952).

¹⁴J. Bevk, J. P. Mannaerts, L. C. Feldman, and B. A. Davidson, *Appl. Phys. Lett.* **49**, 286 (1986).

¹⁵M. W. Muller, *Phys. Rev. B* **30**, 6196 (1984).

¹⁶G. M. Stocks, W. M. Lemmerman, and B. L. Gyorffy, *Phys. Rev. Lett.* **41**, 339 (1978).

¹⁷W. A. Harrison, *Electric Structure and Properties of Solids* (Freeman, San Francisco, 1980).

¹⁸W. A. Harrison, *Microscience* **3**, 35 (1983).

¹⁹The strain energy and the chemical energy can be treated independently since the chemical term does not depend strongly

on bond lengths and thus is not significantly coupled to lattice distortions.

²⁰R. M. Martin, *Phys. Rev. B* **1**, 4005 (1970).

²¹J. C. Mikkelsen, Jr., and J. B. Boyce, *Phys. Rev. Lett.* **49**, 1412 (1982).

²²A. Sher, A.-B. Chen, and M. van Schilfgaarde, *J. Vac. Sci. Technol. A* **4**, 1965 (1986).

²³T. S. Kuan, T. F. Kuech, W. I. Wang, and E. L. Wilkie, *Phys. Rev. Lett.* **54**, 201 (1985).

²⁴A. A. Mbaye, A. Zunger, and D. M. Wood, *Appl. Phys. Lett.* **49**, 782 (1986).

²⁵H. R. Jen, M. J. Cherng, and G. B. Stringfellow, in *Proceedings of the Seventh International Conference on Ternary and Multinary Compounds, Snowmass, Colorado, 1986* (Materials Research Society, Pittsburgh, 1986).

²⁶J. E. Green, *J. Vac. Sci. Technol. B* **1**, 229 (1983).

²⁷R. N. Bicknell, N. C. Giles, J. F. Schetzina, *Appl. Phys. Lett.* **49**, 1095 (1986).

²⁸This is not quite correct since the 12 β force constants connecting those atoms to the central atom also depend on the displacement of the second neighbors. For those β forces we make the assumption predicted by the Shih model (see Ref. 30): that the alloy-C bonds contract by 75% of the difference in the virtual-crystal bond length and the equilibrium bond length. The total energy is quite insensitive to this approximation, and the error is of the order of 1% of the total strain energy.

²⁹Small terms in β , second and higher order, are neglected. Their neglect incurs errors of order 1%.

³⁰K. C. Shih, W. E. Spicer, W. A. Harrison, and A. Sher, *Phys. Rev. B* **31**, 1139 (1985).